

# Experimental Validation of Compliance Models for LADD Transmission Kinematics

G. Mennitto and M. Buehler

Centre for Intelligent Machines, Department of Mechanical Engineering  
 McGill University  
 Montreal, Quebec, H3A 2A7

## Abstract

We introduce new compliance models for LADD transmissions which reduce, by an order of magnitude, inelastic model errors of up to 18% full scale over force and position operating ranges. Elastic models introduced so far were all based on fiber elasticity, which show an increase in LADD length from the inelastic length with force. We show that in experiments the opposite is true. The LADD is always shorter than predicted from the inelastic model. As the load force increases, the LADD length approaches the inelastic length. We found the cause for this fundamentally different elastic behavior to be fiber bending. We also employ one of the new models to improve the prediction of the kinematics of a CLADD, which consists of two concentric LADD devices. The new LADD models are essential for the design of LADD based systems, the online estimation of LADD forces, and accurate control.

## 1 Introduction

A LADD (Linear-to-Angular Displacement Device) is a transmission for converting rotational to translational motion, and is the brainchild of S. C. Jacobsen [3]. The basic element of a LADD is the single cell which consists of two rings joined by high strength fibers as shown in Figure 1. The behavior of this single cell describes the LADD's basic operating characteristics: As the cell is twisted, the distance between the rings decreases, thus rotary motion is translated to linear motion. Conversely, if a twisted cell is subjected to a linear displacement it will unwind, producing rotation. The key advantages of LADDs compared to more traditional transmissions like gears or ball screws are their high strength, low weight, high efficiency, absence of lubricants, and low cost [8]. In addition, they could be manufactured inexpensively. Furthermore, LADD based systems integrate very well along robotic limbs in a similar fashion as muscles do in biological systems and thus result in tight packaging. These properties make LADD systems highly attractive in both robotics and prosthetic applications ([7, 8]).

Concentric LADD (CLADD) transmissions are composed of two sizes of multi-stage LADDs placed coaxially inside one another as shown in Figure 2. In a CLADD actuator system, a stationary motor drives

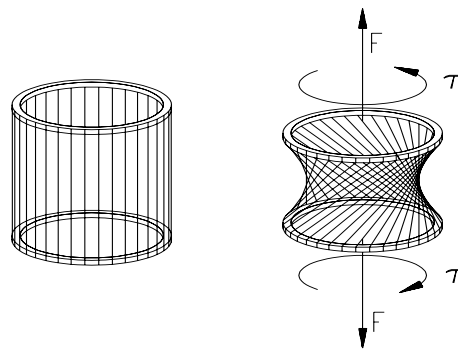


Figure 1: LADD cell. Fully extended, and contracted under a load  $F$  maintained by a torque  $\tau$ .

(rotates) one end of the inner LADD. The remaining end of the inner LADD is rigidly connected to one end of the outer LADD. At this connection point the inner and outer LADDs rotate and translate together; this connection is also where the external load is applied. The remaining end of the outer LADD is fixed (no rotation or translation) at a position close to the motor.

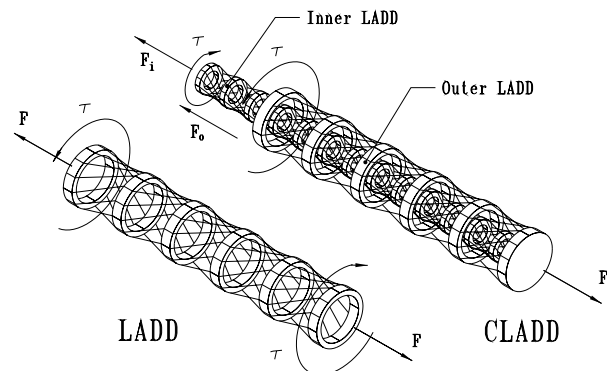


Figure 2: LADD and CLADD.

The major advantage of a CLADD over the single LADD chain is the elimination of the linear slider

mechanism at the load end which is necessary to maintain the torque differential across the cells. Instead, the reaction torque of the CLADD cells occurs near the motor where the torque was initially generated. Now the load end of the CLADD must be permitted to rotate freely which can be accommodated by a cable.

Research on LADDs began with Jacobsen's pioneering work [4, 5, 7, 6]. The importance of modeling LADD compliance for positional accuracy and dynamic performance was already pointed out in [7], but in contrast to our findings, the cause was solely attributed to fiber elasticity. Carruth's thesis [1] reviewed the (non-elastic) kinematics and discussed tradeoffs of different LADD arrangements. Tzeng [12] studied the static and dynamic LADD characteristics by linearizing about equilibrium states to investigate natural frequencies, mode shapes and frequency response characteristics. The dynamic inelastic and elastic models for a concentric LADD were developed in [10, 11]. That particular model was again based on fiber elasticity, and was not experimentally verified.

## 2 Inelastic C/LADD Models

### LADD Model

The inelastic model relating LADD length  $l$  versus input rotation  $\theta$  is readily derived from its geometry, depicted in Figure 3. The cell fiber links are assumed to remain straight and of constant length  $L$  during cell rotation.

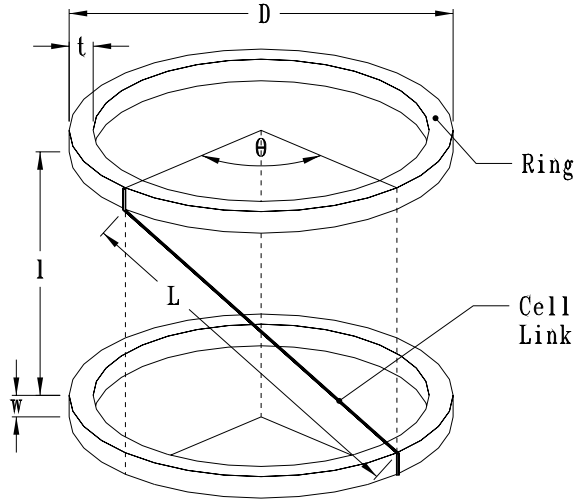


Figure 3: *Inelastic LADD model cell geometry. This model assumes that the cell fiber link remains straight and of constant length  $L$  during cell rotation.*

Keeping the lower ring fixed and rotating the upper ring by  $\theta$ , the upper fiber ends displace by  $D \sin \frac{\theta}{2}$ . With  $L^2 = l^2 + D^2 \sin^2(\frac{\theta}{2})$ , and solving for the cell length  $l$ , we get  $l(\theta) = D \sqrt{\mu^2 - \sin^2(\frac{\theta}{2})}$ , where  $\mu \stackrel{\text{def}}{=}$

$L/D$  is the cell's aspect ratio. A chain of  $n$  cells will equally divide the input rotation  $\theta$ , giving the  $n$ -cell LADD kinematics as

$$l(\theta) = nD \sqrt{\mu^2 - \sin^2(\frac{\theta}{2n})} \quad (1)$$

and where the contraction from full extension is

$$\Delta l(\theta) = nD \sqrt{\mu^2 - \sin^2(\frac{\theta}{2n})} - nL. \quad (2)$$

Referring to Figures 2 and 3, the transmission ratio or lead  $r(\theta)$  of a LADD can be derived from the principle of virtual work  $dW = F dl + \tau d\theta = 0$  and the derivative of (1)  $dl/d\theta$ , as

$$r(\theta) \stackrel{\text{def}}{=} \frac{\tau}{F} = -\frac{dl}{d\theta} = \frac{D \sin \frac{\theta}{n}}{4 \sqrt{\mu^2 - \sin^2(\frac{\theta}{2n})}}. \quad (3)$$

### CLADD Model

In CLADD design, the coaxial positioning of the inner LADD with respect to the outer requires that both LADDs contract by the same amount. Their lengths are given by (1) as

$$l_i = n_i D_i \sqrt{\mu_i^2 - \sin^2(\frac{\theta_i}{2n_i})}, \quad l_o = n_o D_o \sqrt{\mu_o^2 - \sin^2(\frac{\theta_o}{2n_o})}$$

where subscripts  $i$  and  $o$  denote the inner and outer LADDs respectively. Since each LADD is made of equal length, the full length of both LADDs and thus the CLADD is  $l^o$ , where

$$l^o = n_i D_i = n_o D_o. \quad (4)$$

Further simplification is introduced by giving both LADDs an aspect ratio of unity,

$$\mu_i = \frac{L_i}{D_i} = \mu_o = \frac{L_o}{D_o} = 1. \quad (5)$$

Using (4) and (5), the individual LADD models simplify to

$$l(\theta_i) = l^o \cos \frac{\theta_i}{2n_i}, \quad l(\theta_o) = l^o \cos \frac{\theta_o}{2n_o}. \quad (6)$$

Since both LADDs are in parallel, the contraction lengths of the inner and outer LADDs are identical, and therefore, from (6),

$$\frac{\theta_i}{n_i} = \frac{\theta_o}{n_o}. \quad (7)$$

The total input rotation  $\theta$  of the driving source, the motor, is shared by both LADDs,  $\theta = \theta_i + \theta_o$ . Substituting into equation (7), we get

$$\theta_i = \frac{\theta n_i}{n_i + n_o}, \quad \theta_o = \frac{\theta n_o}{n_i + n_o}. \quad (8)$$

Now, from (6) and (8) the CLADD model is

$$l(\theta) = l^o \cos \frac{\theta}{2(n_i + n_o)} \quad (9)$$

and the change in length from full extension is

$$\Delta l = l^o \left( \cos \frac{\theta}{2(n_i + n_o)} - 1 \right). \quad (10)$$

As with a LADD, the load  $r(\theta)$  for a CLADD can be derived from the principle of virtual work  $dW = Fdl + \tau d\theta = 0$  and the derivative of (9)  $dl/d\theta$  as

$$r(\theta) \stackrel{\text{def}}{=} \frac{\tau}{F} = -\frac{dl}{d\theta} = \frac{l^o}{2(n_i + n_o)} \sin \frac{\theta}{2(n_i + n_o)}. \quad (11)$$

The load distribution over the two LADDs is given as

$$F_i = \frac{2\tau}{D_i \sin \frac{\theta}{2(n_i + n_o)}} \quad \text{and} \quad F_o = \frac{2\tau}{D_o \sin \frac{\theta}{2(n_i + n_o)}},$$

where  $F_i + F_o = F$ .

We designed and built two CLADDs based on the models presented above for the development of an antagonistic LADD actuation system [9]. The outer (inner) LADDs consisted of 15 (30) cells with link length of 16 (8) mm and a cell diameter of 16 (8) mm. In order to verify LADD models, repeatable experiments are a basic prerequisite. From preliminary experiments with a test LADD, we found two dominant “break-in” phenomena which effect repeatability. The first one, fiber creep, is the non-elastic (plastic) stretching of a fiber under load. The second effect, glue shaping, is caused when the cell fiber links slowly work away the corners of the glue that bond them to the LADD rings and end pieces. Both effects can be minimized by proper break-in procedures, described in [8]. However, both effects show non-vanishing steady state changes, which, though small, may account for the current modeling limits.

### Experimental Setup

Kinematic validation of the LADDs involved testing them under a variety of static loads with the experimental set-up illustrated in Figure 4. It consists of a linear arrangement of a motor, coupled to a thrust bearing assembly to drive the LADD or CLADD, a linear motion guide, two pulleys and the load. For CLADD testing the linear motion guide was removed. The motor and the large pulley are instrumented to measure the LADD input angle and the LADD linear displacement, respectively. The motor torque is available as a feedback signal from the servo amplifier.

### C/LADD Model Validation Results

The kinematic relationship between motor input angle and LADD length is problematic. The experimental contraction length  $dl$  is plotted with the in-elastic LADD model (2) in Figure 8. We obtain a full

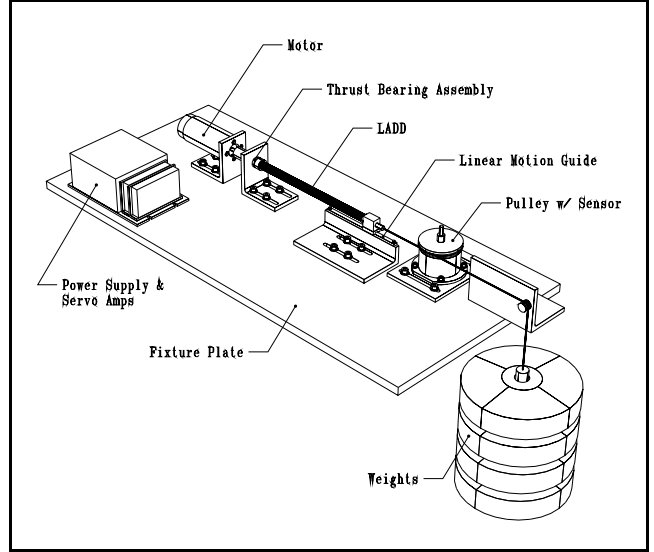


Figure 4: *Experiment set-up.*

scale model difference of 18.3% at a 1kg load and 9.2% at a 35kg load. As the motor angle  $\theta$  increases, the magnitude of error increases as well and in contrast, as the load  $F$  increases, the error reduces. The other LADDs illustrate the same behavior with similar errors. Clearly an error of almost 20% is not acceptable as a basis for design and control with LADDs.

Similar kinematic validation experiments were conducted on a CLADD shown in Figure 9. As for the LADD, the theoretical model fails to match the experimental data by as much as 20% full scale, and the error is a function of both input angle as well as load. Again, an improved model is necessary.

## 3 New LADD Model

The results from the previous model validation section establish a clear need for a compliance model, since the modeling error is directly related to the applied load. While previous work on compliant models [7, 11] simply attributed this to fiber elasticity, both our experiments with fiber creep [8] and others [2] show that the fibers’ high stiffness cannot account for this effect.

### Fiber Bending

A close look at a LADD cell in operation shows that the fibers have a finite curvature at the boundaries to the rings, as illustrated in Figure 5. This contradicts the inelastic model’s assumption that LADD cell fiber links remain straight during operation. We observe that fiber bending becomes more apparent at large cell twist angles and reduces under high LADD loads. This reflects the increasing modeling errors at large angles and decreasing modeling errors at large forces as shown in Figures 8 and 9. Thus we are motivated to include a force dependent “fiber bending term,”

captured in the ‘‘Local Compliance Model,’’ described below.

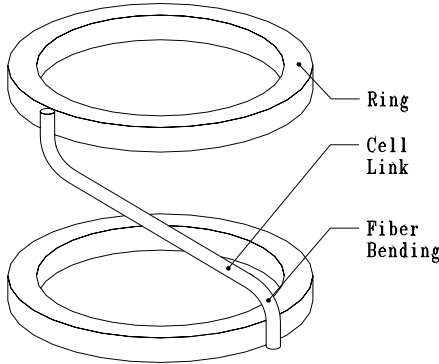


Figure 5: Cell fiber link bending at its boundaries.

### 3.1 Local Compliance Model (LCM)

The LCM identifies an effective fiber link length  $L$  as a function of both LADD angle  $\theta$  and load  $F$ . It is titled ‘‘local’’ because it addresses the previously identified modeling problem due to fiber bending at the source, locally at the level of the individual cell kinematics, before the overall LADD kinematics are developed. Motivated by the particular form of the errors (see Figure 6) between the inelastic model and experiments,  $L(\theta, F)$  was chosen to be of the form

$$L(\theta, F) = L^\circ - a(F) \frac{\theta^2}{n^2}, \quad a(F) = b_1 \exp^{b_2 F} + b_3 \quad (12)$$

where  $L^\circ$  is the design cell length.

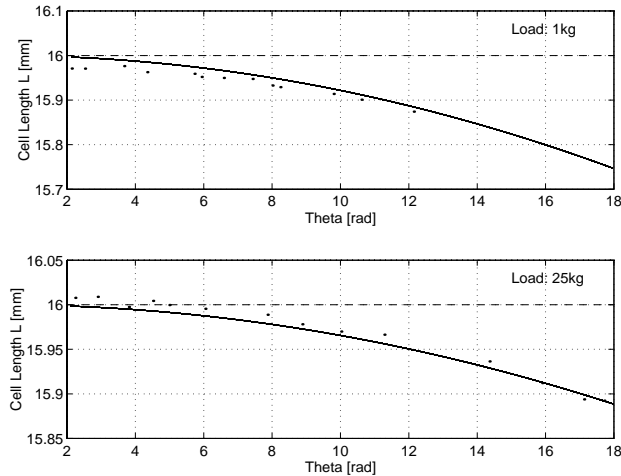


Figure 6: Effective fiber link length  $L(\theta, F)$  for a LADD cell from the Local Compliance Model given by (12) (solid line) plotted with experimental data ( $\cdot$ ). The dashed line shows the design cell length  $L^\circ$ .

Using the same approach as the inelastic LADD model, we derive the kinematic and static relations of

the LCM as

$$l(\theta, F) = n \sqrt{(L^\circ - a(F) \frac{\theta^2}{n^2})^2 - D^2 \sin^2(\frac{\theta}{2n})} \quad (13)$$

and

$$\frac{\tau}{F} = -\frac{dl}{d\theta} = \frac{2a(F) \frac{\theta}{n} (L^\circ - a(F) \frac{\theta^2}{n^2}) + \frac{D^2}{4} \sin \frac{\theta}{n}}{\sqrt{(L^\circ - a(F) \frac{\theta^2}{n^2})^2 - D^2 \sin^2(\frac{\theta}{2n})}}. \quad (14)$$

Rewriting the inelastic LADD model kinematics (1) as

$$L(\theta, F)_{exp} = \sqrt{(\frac{l_{exp}}{n})^2 + D^2 \sin^2(\frac{\theta_{exp}}{2n})} \quad (15)$$

we know, from experimental data, the effective cell link length as a function of both LADD angle  $\theta$  and load  $F$ . We then find the coefficients  $b_i$  in (12) by curve fitting to experimental data (see Figure 7).

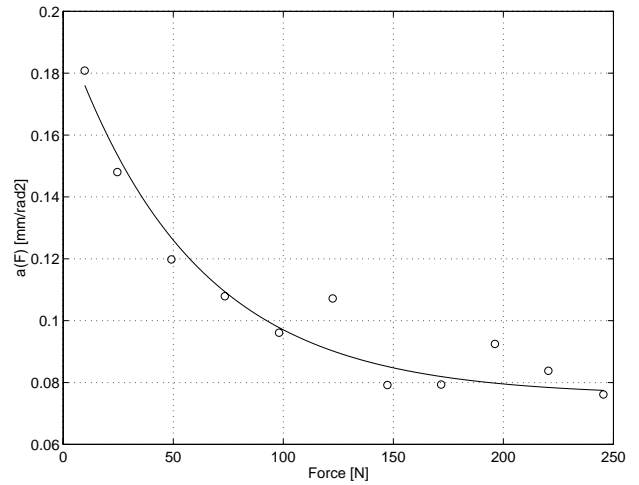


Figure 7: Local Compliance Model  $a(F)$  for a LADD cell. The LCM identifies an effective fiber link length  $L$  given as  $L(\theta, F) = L^\circ - a(F)(\theta/n)^2$ . The data from constant load experimental runs ( $\circ$ ) is fitted to  $a(F) = b_1 \exp^{b_2 F} + b_3$  (solid line).

The improvements, shown in Figure 8 are dramatic: The worst case error was decreased from 18.3% full scale to 1.3% over the entire load and angle range! We have thus developed and verified an improved model, paying attention to the physical realities. Given the resulting complex model, the question arises: Can we simplify the model and still maintain accuracy? This question is answered in the next section.

### 3.2 Global Compliance Model (GCM)

The GCM identifies a global compliance term  $g(F)$ . It is considered ‘‘global’’ because it attempts to improve modeling by multiplying the overall contraction LADD length (2) by a factor that accounts for fiber bending as a function of LADD loading. Unlike the

LCM, the GCM is developed after the inelastic model is developed, and is of the form

$$\Delta l(\theta, F) = \Delta l(\theta)_{inelastic} g(F) \quad (16)$$

where

$$g(F) = a_1 \exp^{a_2 F} + a_3 \quad (17)$$

and the coefficients  $a_i$ ,  $i = 1, 3$ , are determined using curve fits to experimental data as above. We derive the lead  $r(\theta)$  as

$$r(\theta, F) \stackrel{\text{def}}{=} \frac{\tau}{F} = -\frac{dl}{d\theta} = \frac{D \sin \frac{\theta}{n}}{4 \sqrt{\mu^2 - \sin^2(\frac{\theta}{2n})}} g(F). \quad (18)$$

For each constant load run, we used the experimental data and inelastic model predictions with least squares to evaluate a single value for  $g(F)$  for (16). By evaluating respective  $g(F)$ s for various loads, the coefficients to (17) were evaluated through curve fitting. The results for this simplified global compliance model (GCM) are shown in Figure 8. Surprisingly, with 1.5% the accuracy is only minimally worse than that of the physically motivated and more complex LCM. Therefore we prefer to use the simpler GCM for further modeling efforts.

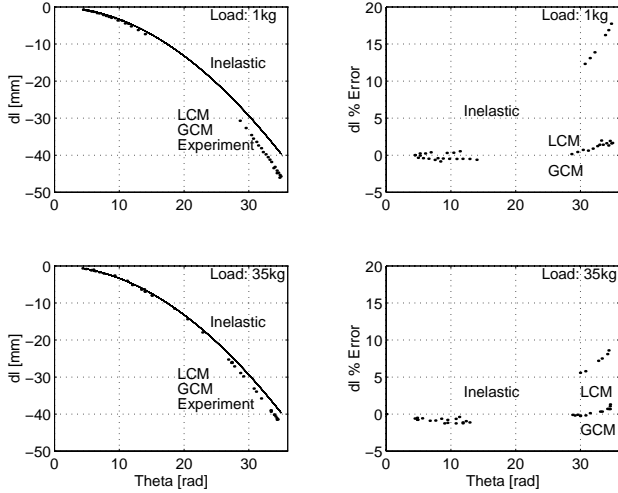


Figure 8: *LADD Kinematics.* The experimental contraction  $dl$  (·) is plotted against the inelastic LADD model (solid line) given by (2). The maximum full scale model difference is 18.3% at a 1kg load (top) and 9.2% at a 35kg load (bottom). As the motor angle  $\theta$  increases, the error increases as well and in contrast, as the load  $F$  increases, the error reduces. Both LCM and GCM models are indistinguishable from the experimental data. The plots on the right show an error reduction down to 1.5% full scale independent of the applied load.

#### 4 New CLADD Model

The new CLADD model is developed similarly as presented in Section 2. From (16) the change in

lengths for each LADD, assuming the outer and inner LADDs are made to be of equal length at zero relative rotation, is given as

$$\Delta l_i = (n_i D_i \sqrt{\mu_i^2 - \sin^2(\frac{\theta_i}{2n_i})} - n_i L_i) g_i(F_i)$$

and

$$\Delta l_o = (n_o D_o \sqrt{\mu_o^2 - \sin^2(\frac{\theta_o}{2n_o})} - n_o L_o) g_o(F_o).$$

Equating the contraction length of the inner to that of the outer and giving both LADDs an aspect ratio of unity, simplifies to

$$(\cos \frac{\theta_i}{2n_i} - 1) g_i(F_i) = (\cos \frac{\theta_o}{2n_o} - 1) g_o(F_o). \quad (19)$$

Unlike the simple CLADD model presented in Section 2, we are not able to obtain a simple relation between  $\theta_i$  and  $\theta_o$ . As before, the total input rotation  $\theta$  of the driving source, the motor, is shared by both LADDs,

$$\theta = \theta_i + \theta_o. \quad (20)$$

In addition, we have

$$F = F_i + F_o. \quad (21)$$

The load distribution over the two LADDs is given as

$$F_i = \frac{2\tau}{D_i \sin \frac{\theta_i}{2n_i} g_i(F_i)} \quad (22)$$

and

$$F_o = \frac{2\tau}{D_o \sin \frac{\theta_o}{2n_o} g_o(F_o)}. \quad (23)$$

To verify the model we solve numerically the set of equations (19), (20), (21), and either (22) or (23) using experimental data for  $\theta$ ,  $F$ ,  $\tau$ . The results are shown in Figure 9. For large loads of 50kg both the inelastic model (10), as well as our new CLADD model derived from the two LADDs' GCM model are within 3% of the experimental data. But again, just like with the individual LADDs, the differences increase with decreasing load, since the fiber bending effect is increasing. At a load of 10kg, for example, the inelastic CLADD model results in a worst case error of 20%. In contrast, with our new model, the error is substantially reduced, and remains bounded to within 5%.

A global CLADD model could be identified, which might match the experimental data even better. However, such a model won't let us derive the load distribution for individual LADDs, which is necessary to monitor the individual LADD's operating conditions. On the other hand, one might ask why our model is not predicting the CLADD response better, being built upon LADD models which are accurate to within

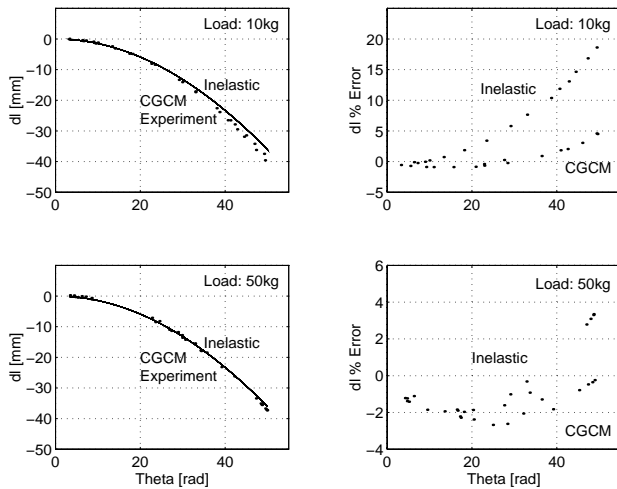


Figure 9: *CLADD Kinematics*. The inelastic *CLADD* model (solid line) given by (10) is plotted together with experimental contraction  $dl$  of a *CLADD* and our new model based on the individual *LADDs*' *GCM*.

1.5%. Besides the additive nature of both *LADD* models' inaccuracies, the main cause can almost certainly be attributed to our novelty to *LADD* manufacturing: the inner *LADD* is a small amount longer than the outer *LADD* – the *CLADD* thus violates assumption (4). A better match between inner and outer *LADD* length should further improve our model's accuracy.

## 5 Conclusion

Based on our experimental work with *LADDs*, we have identified a substantial error between the traditionally used inelastic kinematic model based on a simple geometric derivation and the experimentally observed data. We have identified the underlying effect to be not fiber elasticity, but fiber bending. Two new compliance models, a Local Compliance Model (*LCM*) and a Global Compliance Model (*GCM*) were introduced, one of them modeling the fiber bending effect explicitly. Both models resulted in a reduction of the worst case error of an order of magnitude.

With our improved knowledge about *LADDs*' properties, their manufacturing challenges, and more accurate models, these interesting devices could find many applications in electrically actuated autonomous systems or any other motion control application where weight is critical.

## References

- [1] J. C. Carruth. Operations characteristics of the *LADD* actuator. M. Eng. Thesis, University of Utah, 1975.
- [2] A. Nahvi et al. An investigation of the transmission system of a tendon driven robot hand. In *Proc. IEEE/RSJ Conf. Intelligent Systems and Robots*, pages 202–208, Munic, Germany, Sep 1994.

- [3] S. C. Jacobsen. Rotary-to-linear and linear-to-rotary motion converters. US Patent 3864983, 1975.
- [4] S. C. Jacobsen and R. B. Jerrard. Torsion of Rope-Connected Hoops Leads to Light Weight Prosthetic Actuator. In *26th ACEMB*, Sep 1973.
- [5] S. C. Jacobsen, R. B. Jerrard, and D. Knutti. Preliminary Report on the Utah Arm. In *Conference on Engineering Devices in Rehabilitation*, Boston, MA, May 1974.
- [6] S. C. Jacobsen, R. B. Jerrard, and D. Knutti. Development and Control of the Utah Arm. In *Proc. of 5th Int. Symp. on External Control of Human Extremities*, Dubrovnik, Yugoslavia, Aug 1975.
- [7] S. C. Jacobsen, R. B. Jerrard, D. Knutti, and J. Carruth. The Ladd Actuator as a Prosthetic Muscle. In *Proc. of 5th Int. Symp. on External Control of Human Extremities*, Dubrovnik, Yugoslavia, Aug 1975.
- [8] G. Mennitto. Compliant articulated robot leg with antagonistic *LADD* actuation. M.Eng. Thesis, McGill University, Feb 1995.
- [9] G. Mennitto, P. Gregoire, and M. Buehler. CARL: A Compliant Articulated Robotic Leg for Dynamic Locomotion. In *Int. Conf. Intelligent Autonomous Systems, IAS-4*, pages 702–707, Karlsruhe, Germany, Mar 1995.
- [10] K. L. Pottebaum. *Dynamic nonlinear inelastic and elastic models for a concentric LADD actuator*. PhD thesis, University of Texas at Austin, 1982.
- [11] K. L. Pottebaum and J. J. Beaman. A dynamic model of a concentric *LADD* actuator. *ASME J. Dynamics Systems, Measurement, and Control*, 105:157–164, Sep 1983.
- [12] S. K. Tzeng. *The static and dynamic characteristics of LADD actuators*. PhD thesis, The University of Texas at Austin, 1980.